



Development and electrochemical studies of membrane electrode assemblies for polymer electrolyte alkaline fuel cells using FAA membrane and ionomer

Marcelo Carmo^{a,1}, Gustavo Doubek^{a,b,2}, Ryan C. Sekol^a, Marcelo Linardi^b, André D. Taylor^{a,*}

^a Chemical & Environmental Engineering Department, Yale University, 9 Hillhouse Ave, New Haven, CT 06511, USA

^b IPEN – University of São Paulo, São Paulo – SP, Brazil

H I G H L I G H T S

- ▶ Guidelines on the fabrication and operation of HEM fuel cells.
- ▶ Discussion of electrode kinetic parameters and its assembly impacts.
- ▶ Provides criteria for optimized operation of commercially available GDL materials.
- ▶ Relationship between nature of ionomer and reaction resistance within the catalytic layer.

A R T I C L E I N F O

Article history:

Received 9 August 2012
 Received in revised form
 20 November 2012
 Accepted 4 December 2012
 Available online 12 December 2012

Keywords:

Alkaline fuel cell
 Membrane electrode assembly
 FAA
 Solid polymer electrolyte
 Tafel study

A B S T R A C T

This paper provides guidelines on the fabrication and operation of alkaline fuel cells using quaternary ammonium hydroxide anion exchange membrane (FAA-3 – fumatech), and includes a discussion of the electrode kinetic parameters based on the composition of the catalytic layer. The best peak power density performance, 223 mW cm^{-2} was obtained with an electrode formed from Pt/C, $0.8 \text{ mg}_{\text{Pt}} \text{ cm}^{-2}$ and 25% of FAA-3 ionomer in the catalyst layer for both the cathode and the anode. We demonstrate that the platinum loading can be lowered to values close to $0.5 \text{ mg}_{\text{Pt}} \text{ cm}^{-2}$, without appreciably affecting the fuel cell performance characteristics. The experimental fuel cell data were analyzed using theoretical models of the electrode structure and its kinetics studied over the assembling parameters. We show that most of the electrode systems present limiting currents, with some showing diffusion limitations in the gas channels and/or in the ionomer film covering the catalyst nanoparticles. We also provide some general strategies using Tafel slopes on evaluating the ionomer interaction with the electrode kinetics for the oxygen reduction reaction.

© 2012 Elsevier B.V. All rights reserved.

1. Introduction

Fuel cell designs have dramatically improved during the past decades leading to a standardization over all of its components. However, slow electrode kinetics, CO poisoning of expensive noble-

based electrocatalysts and high costs of electrocatalysts and proton exchange membranes such as Nafion, remain as critical challenges. The search for polymeric electrolyte alternatives to Nafion such as hydroxide exchange membranes (HEMs) has recently received attention [1–3]. By switching from an acidic medium to a basic regime, HEMs have the potential to solve the problems of membrane and catalyst cost while achieving respectable power and energy densities [1,2]. Moreover, in a basic environment the oxygen reduction over-potential can be significantly reduced [3]. Another point to be considered is that HEM fuel cells (HEMFCs) potentially do not have durability issues associated with the formation of carbonate/bicarbonate species as observed in the liquid electrolyte solutions due to CO_2 reactions from the oxidant gas stream at cathodes of classic liquid alkaline fuel cells [1,4]. On the other hand the use of HEMs brings about new design and assembly challenges

* Corresponding author. Chemical & Environmental Engineering Department, Yale University, P.O. Box 208286, New Haven, CT 06520-8286, USA. Tel.: +1 203 432 2217; fax: +1 203 432 4387.

E-mail addresses: m.carmo@fz-juelich.de (M. Carmo), gdoubek@ipen.br (G. Doubek), ryan.sekol@yale.edu (R.C. Sekol), andre.taylor@yale.edu (A.D. Taylor).

¹ Present address: Forschungszentrum Jülich GmbH, Institute of Energy and Climate Research, Wilhelm-Johnen-Straße, Jülich 52428, Germany.

² Present address: IPEN, 2242 Ave. Prof Lineu Prestes, Cidade universitária, São Paulo – SP, Brazil.

that should be addressed in order to realize a system that can meet today's requirements in terms of catalyst utilization, performance, and durability. More controllable deposition techniques such as LBL [5], ink-jet printing [6,7], or Tandem Meyer Rod Coating techniques [8] could also provide an extra tool to overcome engineering issues on composing an effective triple-phase reaction site thus enabling improved catalyst utilization of the HEM system [6,9].

Despite the reported degradation mechanisms associated with HEMs such as elimination of a tertiary amine, Stevens rearrangement, rearrangement of the methyl group, and Sommelet – House rearrangement [10], the technology maturation is already strengthening this new research area on conceiving fuel cells working with HEMs [2–4,11]. The most commonly used material for the HEMs is a quaternary ammonium hydroxide containing polymer [2–4,12–24]. This structure provides OH^- mobility by the positively charged nitrogen which is stabilized by the four linked organic groups. The nature and size of the organic groups also define the charge intensity on the nitrogen atom, the pathway for the hydroxide ions, the stability of the membrane against chemical reactions and other membrane properties such as dimensional swelling, ion selectivity and fuel crossover. Presently, Tokuyama, Acta SpA, and FuMA-Tech GmbH are among the companies that commercially produce HEMs. A few studies have reported the use of an HEM from Tokuyama Co. [2,14,15]. Acta SpA. claims to have developed, an HEM membrane and ionomer (I2), with peak power densities of about 300 mW cm^{-2} ; one of the highest values found in the scientific literature [25]. Recently, FuMA-Tech GmbH started commercially producing a new generation of their HEM named FAA-3. It is claimed in the company portfolio that the FAA-3 membrane has high chemical stability, low dimensional swelling, high selectivity and low area resistance. Previously, several other groups have used the previous FAA HEM system [12,13,26–28], yet from a survey in the literature, there is no apparent consensus on the best strategies for optimization of the MEA assembly parameters. The FAA-3 is 50–55 μm thick, and has an ion exchange capacity of 2 meq g^{-1} . In the $-\text{OH}$ form, with a water uptake of 64 wt% at 25 °C, dimensional swelling of 15% at 25 °C, a T_g of 185 °C, and a specific conductivity of 30 mS cm^{-1} in H_2O at 25 °C [29]. These interesting properties for the FAA-3 HEM and together with previous FAA membrane results from other groups [12,13,26–28] using this commercial membrane makes the FAA-3 a good candidate to be taken as a standard material for the development of our study around quaternary ammonium hydroxide anion exchange membrane for the use in HEMFCs.

In this work electrochemical studies on gas diffusion electrodes prepared using FAA-3 HEM as a standard quaternary ammonium hydroxide anion exchange membrane are reported. The system evaluated the following MEA assembly parameters: (i) the effect of the activation for the device, (ii) the effect of the structure and composition of the catalyst layer (Pt loading, ionomer loading), (iii) the effects of the cell temperature and applied torque for assembly, and (iv) discussion of the kinetic parameters in terms of catalytic layer composition and architecture. Our approach was adapted from a previous study by Gonzalez et al. [43] that was done on proton exchange membrane fuel cell MEAs.

2. Experimental

With thermodynamically favorable reaction rates in an alkaline environment, non-noble catalysts such as Ni and Co could be used to prepare the fuel cell electrodes. However, since the scope of this study is not the development of catalyst systems for alkaline fuel cells, the working electrodes were prepared using a conventional brushing procedure [30] using standard and well studied platinum-on-carbon (Pt/C) catalysts (BASF) 20%. Here we use a carbon paper

substrate with a microporous layer (MPL) – Sigracet BC25 – Ballard, an FAA-3 hydroxyl anion exchange ionomer solution (fumatech, 13.5 wt% in N-methylpyrrolidone (NMP)). To prepare the catalyst layer, a homogeneous suspension was formed from the desired amounts of the Pt/C 20% BASF catalyst and the FAA-3 solution (OH^- form) with NMP as solvent/dispersant. After stirring overnight, the 'ink' was quantitatively deposited on the MPL side of the gas diffusion layer by a hand brushing procedure. After each pass, the solvent/dispersant was evaporated to dryness in a vacuum oven at 50 °C until the desired platinum loading is obtained. The FAA-3 (fumatech) membranes were treated with KOH 1 mol L^{-1} at room temperature for 24 h, and then subsequently washed and stored in ultrapure Milli-Q water. The electrodes were placed on each side of the FAA-3 membranes (without the pressing step, since the FAA-3 membranes are pressure sensitive to degradation), and placed inside the fuel cell unit using PTFE gaskets (thickness 10 μm). The experiments were carried out in an Electrochem FC25 single cell. The cell, with an active electrode area (geometric) of 5 cm^2 , was clamped (with a contact pressure on electrochemical active area of 125 cN m^{-2}) between the gold plated copper plates. Humidification of the reactants was carried out by bubbling the gases through water contained in stainless steel bottles heated at the same temperature as the cell. Measurements of cell potential as a function of current density were made galvanostatically using an Agilent loadbank (N3301A) with an HP 6033-A, and coupled to an Acopian booster with the input and output data being automatically controlled and collected by Labview. Studies for the optimization of the gas flow rates were not performed, nevertheless, in order to avoid mass transport limitations from the feed gases, the fuel cell performance was evaluated at a constant stoichiometric ratio of hydrogen, $\lambda_{\text{H}_2} = 1.5$, hydrogen flow: 200 mL min^{-1} , oxygen flow: 200 mL min^{-1} (100% humidity), and atmospheric pressure.

3. Results and discussion

Here we present a detailed approach taken over the HEM fuel cell system assembly and operational parameters. Theoretical and semi-empirical models are used in the latter sections to determine the most important assembly parameters for FAA-3 quaternary ammonium hydroxide anion exchange membranes. Fig. 1 summarizes a one parameter optimization study in a diagram showing the maximum power density reached for each system. The optimization was made changing one of the parameters at a time using the same configuration for both, the anode and the cathode. We start with the activation parameter at the bottom and move towards the torque study at the top (Fig. 1). The data (Table 1) used to compose Fig. 1 was extracted from polarization curves from each MEA configuration with the adjusted parameter featured at the end of the bar graph. An individual analysis over the influence of each parameter is further discussed. It should be noted that this is not a full factorial experiment, and the parameters could be dependent on each other (i.e. the percent ionomer needed could be different for $0.5 \text{ mg}_{\text{Pt}} \text{ cm}^{-2}$ compared to $0.8 \text{ mg}_{\text{Pt}} \text{ cm}^{-2}$).

3.1. Fuel cell activation optimization

The activation of a fuel cell is an important parameter as it allows the system to reduce the number of "dead" regions or number of unavailable catalytic sites, thus permitting the device to reach its full potential [31]. Therefore, properly activating the electrode allows it to reach an optimal condition for the device that will be carried on throughout the MEA lifetime.

For conventional polymer exchange membrane fuel cells (PEMFCs), there are three main methods to activate the MEA to its

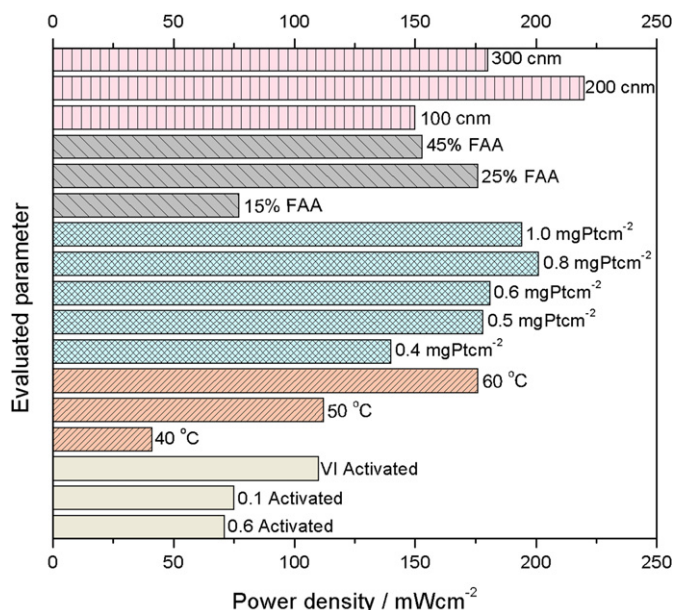


Fig. 1. Summary of all the optimized parameters and its corresponding power density outputs.

best or steady state condition. The first activation technique is the Potentiostatic method, where a potential value is chosen and current is measured overtime. This is typically done by setting the cell potential around 600 mV to give a high power density, or at potential around 100 mV to give a high current density. The high power density is desired to create pathways for ion conductivity between the catalytic layer and the membrane. The high current density is also used to remove possible contaminants present at the catalytic layers. A higher value of the potential or open circuit voltage (around 900 mV) is normally not considered, since it is commonly associated with membrane and catalyst degradation overtime [32,33]. The second activation technique is the Galvanostatic method, where the highest observed current density value is chosen and the resulting increase in potential is observed overtime.

Table 1

Summary of all the optimized parameters and its corresponding power density outputs.

Optimized parameter	Temp (°C)	Anode loading (mg _{Pt} cm ⁻²)	Cathode loading (mg _{Pt} cm ⁻²)	FAA ionomer (wt%)	Torque (cN m)	Peak power density (mW cm ⁻²)
0.6 activated	50	0.5	0.5	25	150	71
0.1 activated	50	0.5	0.5	25	150	75
VI activated	50	0.5	0.5	25	150	110
40 °C	40	0.5	0.5	25	150	41
50 °C	50	0.5	0.5	25	150	112
60 °C	60	0.5	0.5	25	150	176
0.4 mg _{Pt} cm ⁻²	60	0.4	0.4	25	150	140
0.5 mg _{Pt} cm ⁻²	60	0.5	0.5	25	150	178
0.6 mg _{Pt} cm ⁻²	60	0.6	0.6	25	150	181
0.8 mg _{Pt} cm ⁻²	60	0.8	0.8	25	150	201
1.0 mg _{Pt} cm ⁻²	60	1.0	1.0	25	150	194
15% FAA	60	0.8	0.8	15	150	77
25% FAA	60	0.8	0.8	25	150	176
45% FAA	60	0.8	0.8	45	150	153
100 cN m	60	0.8	0.8	25	100	150
150 cN m	60	0.8	0.8	25	150	199
200 cN m	60	0.8	0.8	25	200	223
250 cN m	60	0.8	0.8	25	250	177

The third method is the polarization curve at a low pace. In this method (VI activation) [34] the MEA is activated by discharging at constant current density from zero to a maximum current density with an incremental step of 20 mA cm⁻² every 5 min. Fig. 2 shows the resulting polarization curves taken after 5 h of activation using the potentiostatic and VI method. We have limited our study to use the first and third described methods. All tests were performed with Pt/C BASF 20%, 0.5 mg_{Pt} cm⁻², 25% FAA-3 ionomer, 50 °C, 150 cN m of cell torque and FAA-3 membrane.

We show that the best method to activate the MEA using FAA-3 ionomer and membrane is the VI activation method (Fig. 2). We note that this method was previously used for HEMFCs using TPQOH membranes and an FAA-3 membrane [12]. Using the VI activation method, we show power densities of 110 mW cm⁻² which is 40 mW cm⁻² higher than the potentiostatic method at 600 mV or 100 mV (Fig. 2). During our experiments, we also observed that there is a loss in the performance of the cells starting after 5 h. This loss could be related to the degradation of the membrane associated and/or loss and/or degradation of the ionomer, although a more detailed investigation is needed to address the pointed issue. Also, the used solvent (NMP) has a high vapor pressure, and is very likely to stay adsorbed in the microstructure of the carbon support where it slowly poisons the catalyst surface and decreasing the performance. The development of an ionomer that could be dissolved or dispersed in alcohol- or water-based solutions would be important in order to avoid these problems related to the use of organic solvents.

3.2. Fuel cell operating temperature optimization

Next the temperature influence was investigated (Fig. 3). The obtained polarization curves were accomplished with an electrode with 20 wt% Pt/C BASF, 0.5 mg_{Pt} cm⁻², 25% FAA-3 ionomer, FAA-3 membrane and VI activated at 40 °C, 50 °C and 60 °C. An increase in the temperature of the operation should result in a decrease in membrane resistance and an increase in the rate of degradation of the FAA-3 membrane. Fig. 3 shows an increase in limiting current with increasing temperature, indicating that diffusion problems are less important. This can be associated with a decrease in flooding of the catalyst layer by liquid water, especially in the anode [4]. No values beyond 60 °C were attempted since the HEMs degrade above this point [29].

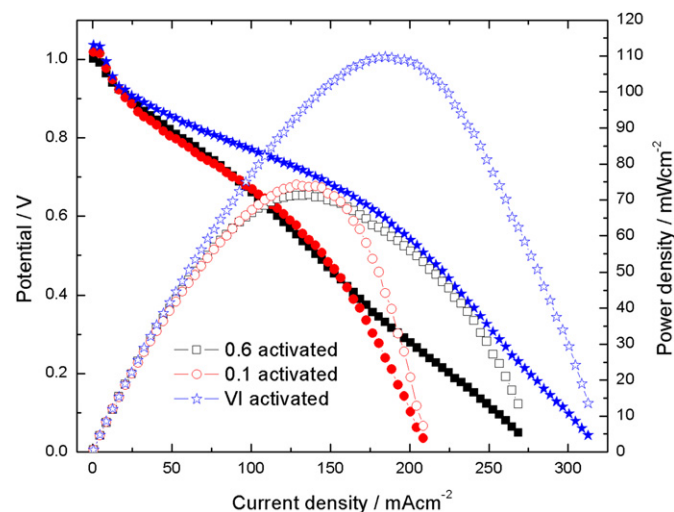


Fig. 2. Polarization curves and power density profiles for the MEAs prepared using different activation methods – analyzing activation method. Closed symbols: potential vs. current density, opened symbols: power density vs. current density.

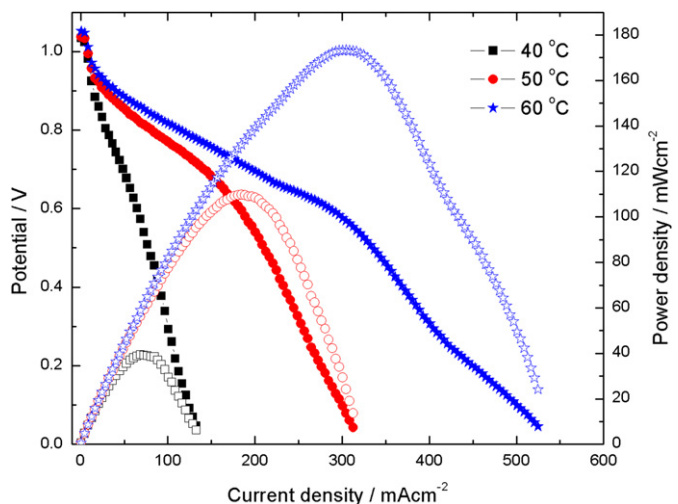


Fig. 3. Polarization curves and power density profiles for the MEAs prepared with FAA-3 membrane and FAA-3 ionomer – analyzing the effect of operating temperature. Closed symbols: potential vs. current density, opened symbols: power density vs. current density.

3.3. Platinum loading optimization

The affect of platinum loading of the catalyst layer is shown in Fig. 4. The electrode with 20 wt% Pt/C containing proportional amounts of FAA-3 in the catalyst layer, with 25% of ionomer over the catalyst content. We show incremental increases of catalyst content of 0.4, 0.5, 0.6, 0.8 and 1.0 $\text{mg}_{\text{Pt}} \text{cm}^{-2}$ (Fig. 1), what corresponded to a proportional loading increase of 25, 20, 33, and 25% at both electrodes. The loading increase resulted in a power density increase in a non-linear fashion, while the first 25% loading increase corresponds to a 25% power increase, the subsequent 100% loading increase only lead to an extra 5% power increase. This demonstrates that in the range 0.5–1 $\text{mg}_{\text{Pt}} \text{cm}^{-2}$, increasing the catalyst loading has a comparatively lower effect on the fuel cell performance. As seen from the comparison of the results on Fig. 4, some expected phenomena were observed as a function of the platinum loading: (i) the values of the experimental open circuit voltage (E_{ocv}) decreased with the decreased catalyst loading, (ii) the linear polarizations are the

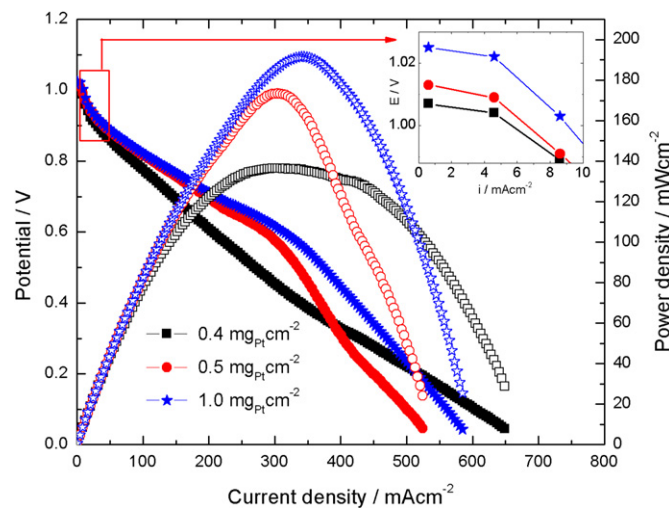


Fig. 4. Polarization curves and power density profiles for the MEAs prepared with FAA-3 membrane and FAA-3 ionomer, (inset: Detailed view of the open circuit voltage) – analyzing catalyst loading. Closed symbols: potential vs. current density, opened symbols: power density vs. current density.

same for loadings down to 0.5 $\text{mg}_{\text{Pt}} \text{cm}^{-2}$, but increase from 0.4 to 0.5 $\text{mg}_{\text{Pt}} \text{cm}^{-2}$. This indicates an increase over the charge transfer resistance which is related to the decrease in the electrochemical active area, when the catalyst loading decreases, (iii) as the loading is increased above 0.8 $\text{mg}_{\text{Pt}} \text{cm}^{-2}$ (data not shown on Fig. 4), some diffusion resistance begins to account for the overall resistance of the cell at higher current densities due to the longer pathway for the gas to diffuse, and therefore decreasing the catalyst utilization at this composition. This statement is further addressed when the fuel cell's resistance is fitted against the theoretical model.

3.4. Ionomer concentration in catalytic layer optimization

When composing a catalytic layer, the ionomer loading is often a key parameter in any PEM fuel cell since it defines the triple-phase boundary and directly influences the catalyst utilization [34–36]. We show that the change of the FAA-3 ionomer loading in the catalytic layer from 15 to 25% appreciably improves the fuel cell performance (Fig. 5). This observation is also reflected by the values obtained for the kinetic parameters when fitted against the theoretical model. However, when the ionomer loading is increased to 45%, a lower peak power density is realized. A lower open circuit voltage and higher linear resistance at 45% loading of FAA-3 ionomer indicate that the catalytic sites have already been covered with adequate amounts of the electrolyte and begin to be super-saturated due to excessive coverage. The electrodes at this stage present the equivalent behavior of a large area flat plate, reaching limiting diffusional currents due to the low solubility of the reactant in the electrolyte.

For FAA-3 ionomer loadings below 1.75 mg cm^{-2} or 25%, an increase in cell's resistance is observed, indicating a decrease of the active area and possibly an increase in the electrolyte resistance. Both phenomena are related to a small amount of FAA-3 impregnated into the electrode, which is insufficient to provide adequate electrolytic conductance inside the catalyst layer, leading to a low platinum utilization and high ohmic drop. This phenomenon is more easily seen when the exchange current densities and the limiting currents are compared. Generally, limiting currents are approximately proportional to the exchange current density, so the same ratio should be expected between

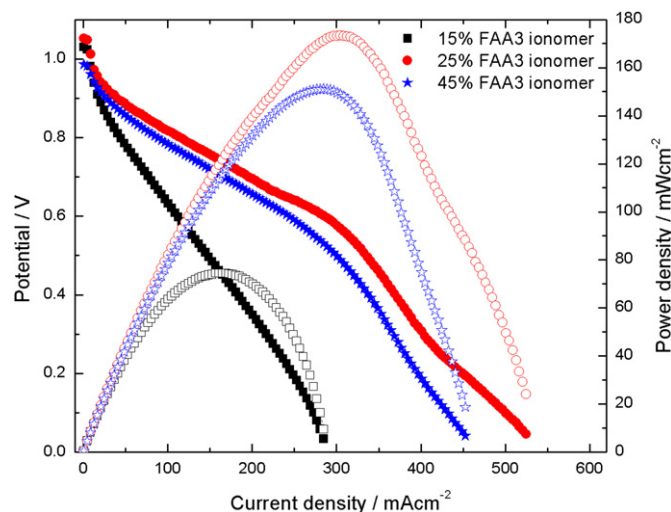


Fig. 5. Polarization curves and power density profiles for the MEAs prepared with FAA-3 membrane and FAA-3 ionomer – analyzing ionomer loading. Closed symbols: potential vs. current density, opened symbols: power density vs. current density.

them at each system [23–29,35]. The exchange current density ratio when moving from 15 to 25% of FAA-3 is ~ 3.5 , but ~ 1.5 for the limiting current. The deviation can be attributed to flooding of the catalyst layer causing difficulty in gas penetration. We note that an increase in ionomer loading, from 25 to 45%, lead to an exchange current density ratio of ~ 1.15 and to a limiting current ratio of ~ 1.2 , indicating a saturation around 25% of ionomer loading, and therefore no higher degree of catalyst coverage by the electrolyte is observed beyond this value. In fact, with lower FAA-3 loadings there is also the possibility for the gases to directly reach the membrane and then to cause a crossover phenomenon. For the highest FAA-3 loading (45%) the slight increase in the cell resistance compared with the value for the optimum condition is possibly related to an excess amount of FAA-3, blocking gas penetration and excessive catalyst coverage leading to a decrease of the catalyst utilization at this composition.

3.5. Fuel cell assembly pressure optimization

To ensure sufficient contact between the catalytic layer and the membrane, the torque applied on the cell assembly was investigated. Table 2 shows the relation between torque and cell resistance (also expressed in terms of power density; Fig. 6). We show a peak power density of 223 mW cm^{-2} at 200 cN m. Below this value the ionomer at the catalytic layer and the membrane are not fully connected whereas above 200 cN m, the FAA-3 membrane starts to lose its structural integrity and leads to a loss on its ionic conductivity. As a comparison, a fuel cell composed of Nafion 212 is pressed with a torque equivalent of 1800 cN m.

3.6. Fuel cell kinetic analysis

Finally all the results provided by the polarization curves were fitted against a theoretical model in order to evaluate separately the cell resistance, the Tafel slope and the open circuit voltage. Eqs. (1) and (2), proposed by Srinivasan et al. [35,37,38], are a semi-empirical model for the representation of the cell potential, E , against current density, i , taking into account the linear resistance due to ohmic processes inside the cell. It was adapted from the theoretical Tafel equation.

Table 2

Kinetic parameters obtained from the fitting of Eq. (1) to the experimental polarization results for the electrodes presenting different characteristics.

Both anode & cathode	E^0/V	$B/\text{V dec}^{-1}$	$R/\Omega \text{ cm}^2$
Temperature ($^{\circ}\text{C}$)			
40	0.882	0.060	5.526
50	0.833	0.071	1.356
60	0.842	0.073	0.981
Catalyst load ($\text{mg}_{\text{Pt}} \text{ cm}^{-2}$)			
0.4	0.847	0.066	1.374
0.5	0.862	0.060	0.981
0.6	0.846	0.068	0.993
0.8	0.846	0.066	0.989
1	0.864	0.064	1.088
Torque on the cell (cN m)			
100	0.835	0.058	0.878
150	0.842	0.058	0.660
200	0.836	0.058	0.603
250	0.838	0.058	0.776
300	0.830	0.058	0.763
Ionomer at catalytic layer (%)			
15	0.850	0.063	2.939
25	0.849	0.070	1.046
45	0.842	0.079	0.988

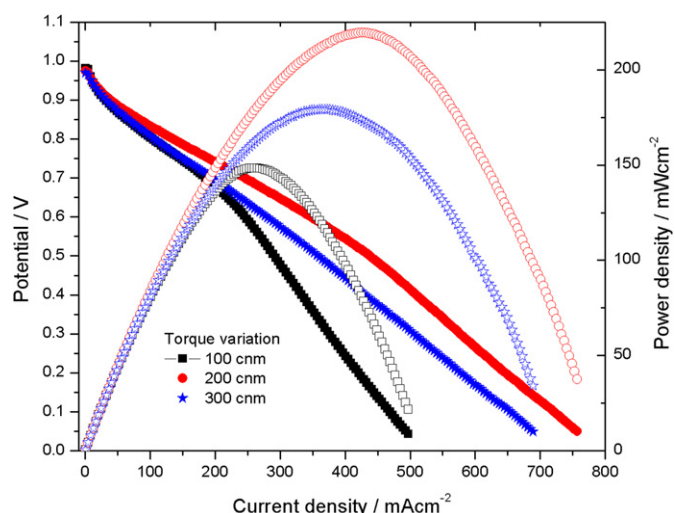


Fig. 6. Polarization curves and power density profiles for the MEAs prepared with FAA-3 membrane and FAA-3 ionomer – analyzing cell assembling pressure. Closed symbols: potential vs. current density, opened symbols: power density vs. current density.

$$E = E^0 - b \log i - Ri \quad (1)$$

$$E^0 = E^r + b \log i_0 \quad (2)$$

where, E^r is the reversible potential for the cell, b is the Tafel slope, i_0 is the exchange current density for the oxygen reduction reaction (ORR), and R represents the overall contributions of the linear polarizations components.

All of the characterizations were fitted against the model using Tafel slope values for the ORR of 2.303 RTF^{-1} above 0.8 V and $2 \times 2.303 \text{ RTF}^{-1}$ below 0.8 V as initial conditions for the fittings [36,39,40]. Table 2 summarizes the kinetic parameters obtained by fitting the model to all of the experimental polarization results.

We can confirm the behavior of the cell resistance as previously discussed for each parameter (Table 2). The temperature increase leads to a decrease over the cell resistance. In the same way, the decrease in the catalyst loading from 0.5 to $0.4 \text{ mg}_{\text{Pt}} \text{ cm}^{-2}$ increased cell resistance from approximately 1 to almost $1.4 \Omega \text{ cm}^2$. We note that for loadings above $0.5 \text{ mg}_{\text{Pt}} \text{ cm}^{-2}$, the cell resistance was almost constant. The ionomer loading leads to an increase over the cell resistance below 25%, going from around 1 to almost $3 \Omega \text{ cm}^2$, but not a significant change above it, further suggests the lack of proper ionomer coverage at the catalytic layer, for values below 25%. The cell reaches an optimal resistance value with a torque around 200 cN m.

We present the calculated Tafel slope (Table 2), which inherently reflects the electrode kinetics. This mainly accounts for oxygen reduction reaction since it is the limiting reaction step [41]. ORR typically presents a value of around 0.06 V dec^{-1} for the Tafel slope, when performed on a platinum flat disc [41]. Since it is obtained for potentials below 0.8 V, there is little influence from cell resistance; therefore a similar value to a full MEA should be expected. As shown in Table 2, the Tafel slope remains constant for most of the studied parameters except for the cell temperature and ionomer loading. The changes related with temperature are expected once the parameter is described by the Tafel slope derived from the Butler–Volmer equation (Eq. (3)) [41].

Table 3

Fitted data from liner scans at different configurations over the same Pt disc electrode recorded in 1 M KOH saturated with oxygen at 1600 rpm.

Tested electrode	E_0 (V)	b (V dec ⁻¹)
Bare Pt disc	0.858	0.058
Pt disc covered with Nafion	0.863	0.057
Pt disc covered with FAA-3	0.847	0.071

$$b = \frac{-2.303RT}{(1 - \beta)nF} \quad (3)$$

where β is the symmetry factor, n the number of exchanged electrons, T the temperature, R the universal gas constant and F the faraday constant.

Although the influence of the ionomer coverage is not explicit in Eq. (3), it is valid to remember that the slope “ b ” usually assumes a symmetry factor of 0.5 that may not be in accordance with the experimental facts. A further analysis into a multi-step reaction as the case of ORR can demonstrate it to be more complex regarding the parameters that can influence the Tafel slope. The electrical work prominent from the electron transfer and the fractions of the total electrical potential difference at the metal interface involved in the charge transfer process might be dependent of the catalyst’s coverage by the electrolyte [42]. In fact, the ionomer’s characteristics such as hydrophobicity, ion conductivity and the particular shape to which the electrolyte allows the arrangement of the ions around it could influence the shape of the double-layer region on which the change in potential and charge transfer reaction occurs at the electrode’s interface. It should be pointed out that complete studies of Tafel slopes in MEAs are very challenging due to large measurements errors, although some empirical equations have been widely used to fit Tafel slope in fuel cells [43]. Nevertheless these results lead us to further investigate this effect in a more controlled environment. This was accomplished using a platinum electrode flat disc in an alkaline solution saturated with oxygen. The Tafel slopes for the oxygen reduction reaction are compared between bare platinum and the same platinum electrode covered with FAA-3 ionomer and also covered with Nafion ionomer. Table 3 shows the average fitted data, according to Eqs. (1) and (2), for four runs at each system for the activation region regarding the reduction of oxygen. The error for the fitted data was 0.5%.

For bare platinum the Tafel slope was calculated as 0.058 which is in accordance with the expected value for this reaction [20–22]. The electrode covered with Nafion presented basically the same slope as the bare platinum indicating a very small structural effect of the Nafion loadings on the polarization behavior, and also in accordance with the results from Gonzalez et al. [43]. The electrode covered with FAA-3 presented significant change over the Tafel slope in accordance with the data derived from the polarization curves from the fuel cell tests presented at Table 2. Although the interference of the ionomer over the Tafel slope is beyond the scope of this study, it raises an interesting engineering parameter towards building an ideal ionomer that does not necessarily need to have the same characteristics of the polymer employed in the ionic exchange membrane.

4. Conclusions

The best performance using the FAA-3 membrane and ionomer for HEMFCs was 223 mW cm⁻² obtained with 20 wt% Pt/C, 0.8 mg_{Pt} cm⁻² and 25% FAA-3 ionomer in the catalytic layer, for both the cathode and anode and 200 cN m of torque. We show that

the platinum requirement can be diminished to values close to 0.5 mg_{Pt} cm⁻² without significant loss of the performance characteristics. We also provide some general strategies using Tafel slopes on evaluating the ionomer interaction with the electrode kinetics for the oxygen reduction reaction, showing that the FAA-3 ionomer, differently from Nafion, seems to have an appreciable influence over it. This systematic study provides basic parameters for HEM fuel MEA evaluation using a commercially available Pt/C catalysts and FAA-3 membrane and ionomer. New ionomer structures and membranes with improved durability will be needed and it is the intent of this manuscript to provide a pathway between catalyst development and the evaluation of HEM fuel cell MEAs.

References

- [1] G.F. McLean, T. Niet, S. Prince-Richard, N. Djilali, International Journal of Hydrogen Energy 27 (2002) 507–526.
- [2] K. Matsuoka, Y. Iriyama, T. Abe, M. Matsuoka, Z. Ogumi, Journal of Power Sources 150 (2005) 27–31.
- [3] E. Antolini, E.R. Gonzalez, Journal of Power Sources 195 (2010) 3431–3450.
- [4] J.R. Varcoe, R.C.T. Slade, Fuel Cells 5 (2005) 187–200.
- [5] F.S. Gittleston, D.J. Kohn, X. Li, A.D. Taylor, ACS Nano 6 (2012) 3703–3711.
- [6] M. Michel, A. Taylor, R. Sekol, P. Podsiadlo, P. Ho, N. Kotov, L. Thompson, Advanced Materials 19 (2007) 3859–3864.
- [7] A.D. Taylor, M. Michel, R.C. Sekol, J.M. Kizuka, N.A. Kotov, L.T. Thompson, Advanced Functional Materials 18 (2008) 1–7.
- [8] X. Li, F. Gittleston, M. Carmo, R.C. Sekol, A.D. Taylor, ACS Nano 6 (2012) 1347–1356.
- [9] A.D. Taylor, E.Y. Kim, V.P. Humes, J. Kizuka, L.T. Thompson, Journal of Power Sources 171 (2007) 101–106.
- [10] M. Tanaka, K. Fukasawa, E. Nishino, S. Yamaguchi, K. Yamada, H. Tanaka, B. Bae, K. Miyatake, M. Watanabe, Journal of the American Chemical Society 133 (2011) 10646–10654.
- [11] E. Agel, J. Bouet, J.F. Fauvarque, Journal of Power Sources 101 (2001) 267–274.
- [12] S. Gu, R. Cai, T. Luo, K. Jensen, C. Contreras, Y. Yan, Chemsuschem 3 (2010) 555–558.
- [13] S. Gu, R. Cai, Y. Yan, Chemical Communications 47 (2011) 2856–2858.
- [14] Z. Ogumi, K. Matsuoka, S. Chiba, M. Matsuoka, Y. Iriyama, T. Abe, M. Inaba, Electrochemistry 70 (2002) 980–983.
- [15] J.R. Varcoe, M. Beillard, D.M. Halepoto, J.P. Kizewski, S.D. Poynton, R.C.T. Slade, ECS Transactions 16 (2008) 1819–1834.
- [16] K.N. Grew, D. Chu, W.K.S. Chiu, Journal of the Electrochemical Society 157 (2010) B1024–B1032.
- [17] M. Kumar, S. Singh, V.K. Shahi, Journal of Physical Chemistry B 114 (2010) 198–206.
- [18] S. Lu, J. Pan, A. Huang, L. Zhuang, J. Lu, Proceedings of the National Academy of Sciences of the United States of America 105 (2008) 20611–20614.
- [19] B.P. Tripathi, M. Kumar, V.K. Shahi, Journal of Membrane Science 360 (2010) 90–101.
- [20] J.R. Varcoe, Physical Chemistry Chemical Physics 9 (2007) 1479–1486.
- [21] G. Wang, Y. Weng, D. Chu, R. Chen, D. Xie, Journal of Membrane Science 332 (2009) 63–68.
- [22] J. Wang, J. Wang, S. Li, S. Zhang, Journal of Membrane Science 368 (2011) 246–253.
- [23] Q. Zhang, Q. Zhang, J. Wang, S. Zhang, S. Li, Polymer 51 (2010) 5407–5416.
- [24] Z. Zhao, J. Wang, S. Li, S. Zhang, Journal of Power Sources 196 (2011) 4445–4450.
- [25] M. Piana, M. Boccia, A. Filpi, E. Flammia, H.A. Miller, M. Orsini, F. Salusti, S. Santiccioli, F. Ciardelli, A. Pucci, Journal of Power Sources 195 (2010) 5875–5881.
- [26] P.V. Mazin, N.A. Kapustina, M.R. Tarasevich, Russian Journal of Electrochemistry 47 (2011) 275–281.
- [27] A. Santasalo-Aarnio, S. Hietala, T. Rauhala, T. Kallio, Journal of Power Sources 196 (2011) 6153–6159.
- [28] Y.S. Yan, S. Gu, R. Cai, T. Luo, Z.W. Chen, M.W. Sun, Y. Liu, G.H. He, Angewandte Chemie International Edition 48 (2009) 6499–6502.
- [29] D. Chen, M.A. Hickner, ACS Applied Materials Interfaces 4 (2012) 5775. <http://dx.doi.org/10.1021/am301557w>.
- [30] W. Vielstich, H. Yokokawa, H.A. Gasteiger, Handbook of Fuel Cells: Fundamentals, Technology, and Applications, In: Advances in Electrocatalysis, Materials, Diagnostics and Durability, Part 1, vol. 5, Wiley, Chichester, West Sussex; Hoboken, NJ, 2009.
- [31] Z. Qi, A. Kaufman, Journal of Power Sources 111 (2002) 181–184.
- [32] K. Teranishi, K. Kawata, S. Tsushima, S. Hirai, Electrochemical and Solid State Letters 9 (2006) A475–A477.
- [33] A. Ohma, S. Suga, S. Yamamoto, K. Shinohara, Journal of the Electrochemical Society 154 (2007) B757–B760.
- [34] M. Boaventura, A. Mendes, International Journal of Hydrogen Energy 35 (2010) 11649–11660.
- [35] E.A. Ticianelli, C.R. Derouin, A. Redondo, S. Srinivasan, Journal of the Electrochemical Society 135 (1988) 2209–2214.
- [36] D.R. Sena, E.A. Ticianelli, V.A. Paganin, E.R. Gonzalez, Journal of Electroanalytical Chemistry 477 (1999) 164–170.
- [37] Y.W. Rho, S. Srinivasan, Y.T. Kho, Journal of the Electrochemical Society 141 (1994) 2089–2096.

- [38] Y.W. Rho, O.A. Velev, S. Srinivasan, Y.T. Kho, *Journal of the Electrochemical Society* 141 (1994) 2084–2088.
- [39] D.B. Sepa, M.V. Vojnovic, L.M. Vracar, A. Damjanovic, *Electrochimica Acta* 32 (1987) 129–134.
- [40] A.J. Appleby, O.A. Velev, J.G. Leheloco, A. Parthasarthy, S. Srinivasan, D.D. Desmarteau, M.S. Gillette, J.K. Ghosh, *Journal of the Electrochemical Society* 140 (1993) 109–111.
- [41] C.H. Hamann, A. Hamnett, W. Vielstich, *Electrochemistry*, Wiley-VCH-Verl., Weinheim, 2007.
- [42] D.S. Gnanamuthu, J.V. Petrocelli, *Journal of the Electrochemical Society* 114 (1967) 1036–1041.
- [43] V.A. Paganin, E.A. Ticianelli, E.R. Gonzalez, *Journal of Applied Electrochemistry* 26 (1996) 297–304.